Does Spectral Nudging Have an Effect on Dynamical Downscaling Applied in Small Regional Model Domains?

BENJAMIN SCHAAF, HANS VON STORCH, AND FRAUKE FESER

Centre for Materials and Coastal Research, Helmholtz-Zentrum Geesthacht, Geesthacht, Germany

(Manuscript received 31 March 2017, in final form 6 July 2017)

ABSTRACT

Spectral nudging is a method that was developed to constrain regional climate models so that they reproduce the development of the large-scale atmospheric state, while permitting the formation of regional-scale details as conditioned by the large scales. Besides keeping the large-scale development in the interior close to a given state, the method also suppresses the emergence of ensemble variability. The method is mostly applied to reconstructions of past weather developments in regions with an extension of typically 1000–8000 km. In this article, the authors examine if spectral nudging is having an effect on simulations with model regions of the size of about 700 km × 500 km at midlatitudes located mainly over flat terrain. First two pairs of simulations are compared, two runs each with and without spectral nudging, and it is found that the four simulations are very similar, without systematic or intermittent phases of divergence. Smooth fields, which are mainly determined by spatial patterns, such as air pressure, show hardly any differences, while small-scale and heterogeneous fields such as precipitation vary strongly, mostly on the gridpoint scale, irrespective if spectral nudging is employed or not. It is concluded that the application of spectral nudging has little effect on the simulation when the model region is relatively small.

1. Introduction

After having observed that the traditional setup of regional climate modeling, namely a relaxation only along a sponge zone at the lateral boundaries, plus a forcing at the lower boundary, exerts an insufficient steering of the large-scale dynamics in the interior of a region of 1000–8000 km, the concept of additionally constraining the large spatial scales of these fields in the interior and above a certain level was introduced. Without this so-called spectral nudging (von Storch et al. 2000; Castro et al. 2005; Rockel et al. 2008a), in the interior different trajectories emerge intermittently in an ensemble of regional simulations (Weisse et al. 2000; Weisse and Feser 2003; Feser and Barcikowska 2012; Giorgi and Bi 2000; Lucas-Picher et al. 2008; Deque et al. 2012; Christensen et al. 2001; Caya and Biner 2004; Laprise et al. 2012).

However, when such a constraint was implemented, the different trajectories stayed close to each other and also close to observations for the entire time. Thus, the advantage of using spectral nudging in regional modeling was to enforce similarity of the large-scale state with a given state and the efficient reduction of ensemble variability. Separovic et al. 2015 showed that the internal variability at scales larger than 300 km can be reduced by using spectral nudging. Recently, such constraining was also used for improving the forecast of regional details (Zhao et al. 2016, 2017). These results were based on simulations with grid sizes of about 20 km and more and domains of 1000 km and more (Feser et al. 2011).

After computer resources further improved, more and more studies of regional models that explicitly resolve convective processes are used for dealing with small-scale atmospheric variability (Prein et al. 2015). For doing so, the grid resolution is significantly reduced to a few kilometers—and at the same time the domain size is reduced to less than 1000 km, say 500 km and less due to high computing time costs for such small grids and time steps. These small regions are quickly flushed by horizontal transports, and it is plausible that in these small-domain cases the lateral boundary value constraints are

Denotes content that is immediately available upon publication as open access.

Corresponding author: Benjamin Schaaf, benjamin.schaaf@hzg.de

DOI: 10.1175/MWR-D-17-0087.1

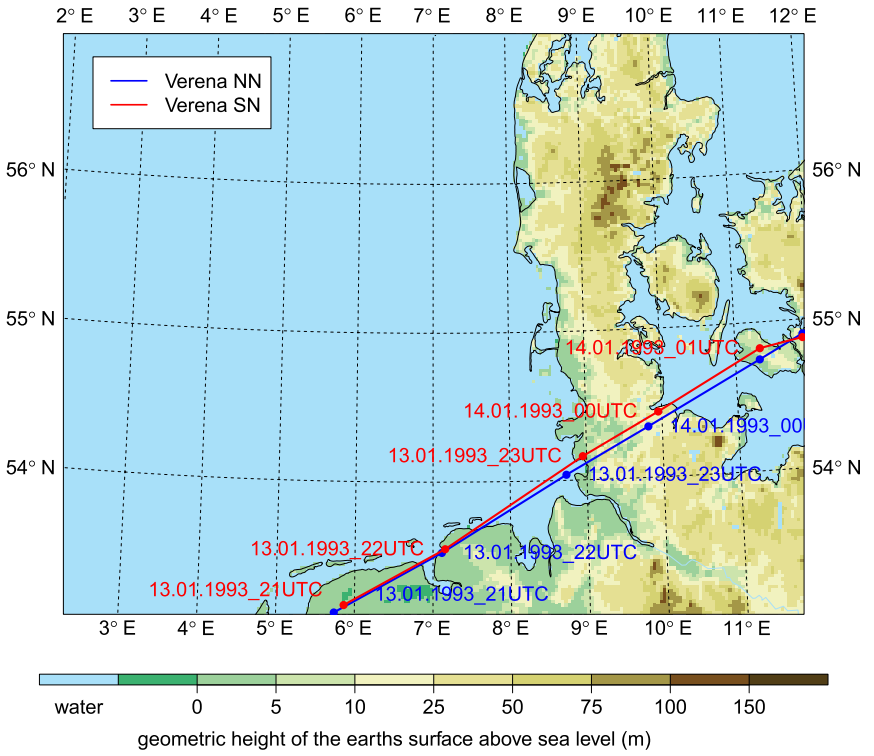

FIG. 1. Model domain of the high-resolution simulation with tracks of storm Verena of January 1993 for SN (red) and NN (blue) simulations.

much more efficient in determining the "large scale" (large compared to the domain size) state within the domain. Therefore the additional constraining by spectral nudging and related techniques in keeping the trajectory close to the prescribed state and the suppression of intermittent divergence in phase space may be of little significance. Our present short article deals with this question. We describe our experimental setup and the evaluation strategy in section 2, in section 3 evidence from our numerical experimentation is presented, and in section 4 we add a short discussion.

2. Experimental setup

a. Simulations

We employ the nonhydrostatic limited-area atmospheric model COSMO-CLM (version 5.0) (Rockel et al. 2008b; Steppeler et al. 2003) (CCLM), which is the climate version of the regional weather prediction model COSMO of the German Weather Service (DWD). The model domain covers the North Sea and northwestern Germany (Fig. 1), with about 700 km in longitudinal direction and about 500 km in latitudinal direction. The grid sizes amount to about 2.8 km; the time step is 25 s. The lateral sponge zone is 12 grid points wide. The simulations are forced by the coastDat II dataset, which is an atmospheric reanalysis for Europe for the last 67 years, from 1948 to 2014 (Geyer 2014; Geyer and Rockel 2013). For the coastDat reanalysis, NCEP–NCAR global reanalysis was dynamically downscaled using the earlier version 4.8 of the same, albeit hydrostatic regional CCLM model to a grid distance of 0.22° (~24 km). Spectral nudging was applied for the horizontal wind components (U, V), beginning at a height level of 850 hPa with exponentially increasing strength toward higher layers. Therefore, the RCM solution in gridpoint space is transformed with a Fourier transformation into the spectral space. The spectral nudging term is then added to the RCM solution for a certain range of wavenumbers while the other wavenumbers are left unchanged. Then the RCM results are transformed back from the spectral space to the gridpoint space. Below 850 hPa no spectral nudging (SN) is applied so that small weather phenomena, which often occur close to the surface, are not affected.

In total, four simulations were computed with this model, all for the year 1993. We chose this year because we expected larger deviations between the ensemble members in this year due to a former study (von Storch

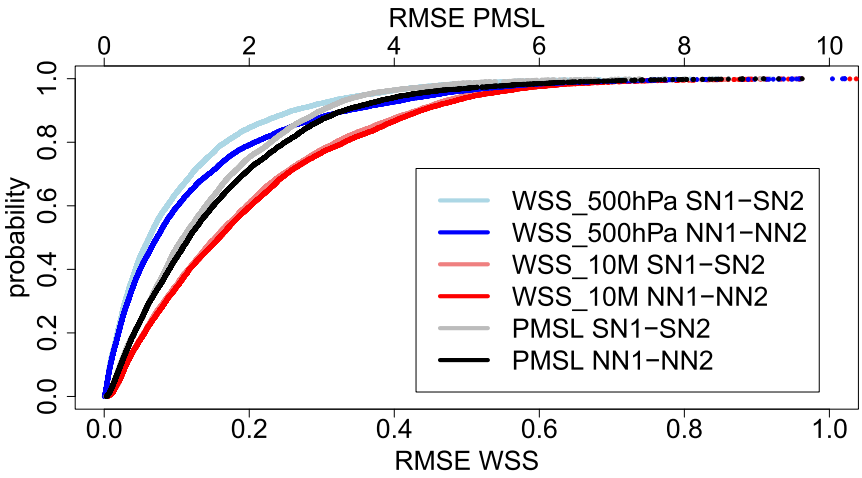

FIG. 2. Distribution function of the RMSE between SN_1 and SN_2 (light color) and between NN_1 and NN_2 (dark color) for 10-m wind speed (red, WSS_10M), sea level pressure (black, PMSL), and wind speed in 500 hPa (blue, WSS_500 hPa).

et al. 2000). This study analyzed the winter 1993 (January–March), during which a major phase of divergence took place, where differences in the large-scale patterns without spectral nudging arose between the nonnudged simulation and the forcing data. The study used a domain of about 5000 km × 4500 km and grid sizes of 53 km. Two simulations, which employed spectral nudging toward the coastDat dataset (SN_1 and SN_2),

TABLE 1. Statistical values of hourly data differences SN_1–NN_1, NN_1–NN_2, and SN_1–SN_2 for 1993 for 10-m wind speed (WSS_10M), total precipitation (TOT_PREC), sea level pressure (PMSL), 500-hPa wind speed (WSS_500 hPa), and 2-m temperature (T_2M). For precipitation, only hourly precipitation sums are considered, which are different from zero. Shown are the absolute maximum difference, the mean difference, the standard deviation, and the 99th percentile of the difference. In addition, the values and dates of the minimal pattern correlation between SN_1 and NN_1, NN_1 and NN_2, and SN_1 and SN_2 are shown. Also, the 10th percentiles of the pattern correlation and the values of the minimum time correlations are listed.

		WSS_10M (m s^{-1})	TOT_PREC (mm)	PMSL (Pa)	WSS_500 hPa (m s^{-1})	T_2M (K)
Absolute max	SN_1–NN_1	17.76	64.53	284	21.69	9.45
	NN_1–NN_2	15.24	38.44	158	15.64	4.97
	SN_1–SN_2	12.79	31.80	146	14.24	9.05
Mean	SN_1–NN_1	−0.01	0	7.41	0.07	0
	NN_1–NN_2	0	0	0	0	0
	SN_1–SN_2	0	0	−0.01	0	0
Std dev	SN_1–NN_1	0.54	0.42	12.13	1.11	0.21
	NN_1–NN_2	0.26	0.21	2.07	0.20	0.09
	SN_1–SN_2	0.25	0.21	1.83	0.16	0.11
99th percentile	SN_1–NN_1	1.62	1.03	41.46	3.18	0.68
	NN_1–NN_2	0.79	0.34	6.66	0.57	0.28
	SN_1–SN_2	0.76	0.33	5.77	0.44	0.39
Min pattern correlation	SN_1–NN_1	0.79	−0.01	0.92	0.39	0.79
	NN_1–NN_2	0.90	0	0.99	0.95	0.91
	SN_1–SN_2	0.92	0	0.99	0.96	0.94
Date (1993) of min pattern correlation	SN_1–NN_1	1700 UTC 11 Jul	1600 UTC 26 Apr	0000 UTC 11 Mar	1400 UTC 13 Apr	1100 UTC 16 Oct
	NN_1–NN_2	1200 UTC 24 Nov	0000 UTC 19 Oct	1600 UTC 18 Sep	0900 UTC 11 Sep	1700 UTC 6 Aug
	SN_1–SN_2	1600 UTC 13 Aug	0100 UTC 21 Nov	0500 UTC 18 Sep	0400 UTC 11 Sep	1300 UTC 16 Oct
10th percentile of pattern correlation	SN_1–NN_1	0.94	0.29	0.997	0.91	0.98
	NN_1–NN_2	0.98	0.68	0.9998	0.99	0.99
	SN_1–SN_2	0.98	0.68	0.9999	0.997	0.99
Min time correlation	SN_1–NN_1	0.96	0.62	0.9998	0.98	0.99
	NN_1–NN_2	0.99	0.84	0.999	0.99	0.997
	SN_1–SN_2	0.99	0.84	0.999	0.99	0.995

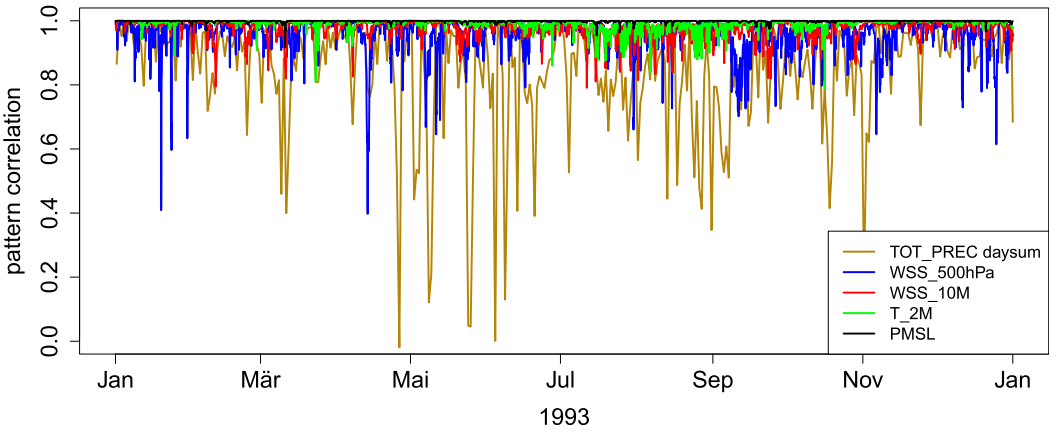

FIG. 3. Time series of the hourly pattern correlation between SN_1 and NN_1 (except for "TOT_PREC daysum" daily values are shown) of sea level pressure (PMSL), 2-m temperature (T_2M), 10-m wind speed (WSS_10M), 500-hPa wind speed (WSS_500 hPa), and the daily sum of precipitation (TOT_PREC_daysum).

and two without spectral nudging (NN_1 and NN_2) were performed. In all four simulations, lateral boundary conditions were relaxed toward the coastDat dataset, using a conventional sponge zone constraint (Davies 1976). One of the SN and one of the nonnudged (NN) simulations were initialized on 1 December 1992 (SN_1 and NN_1); the other two were initialized on 1 November 1992 (SN_2 and NN_2). Previous experiments showed that such a

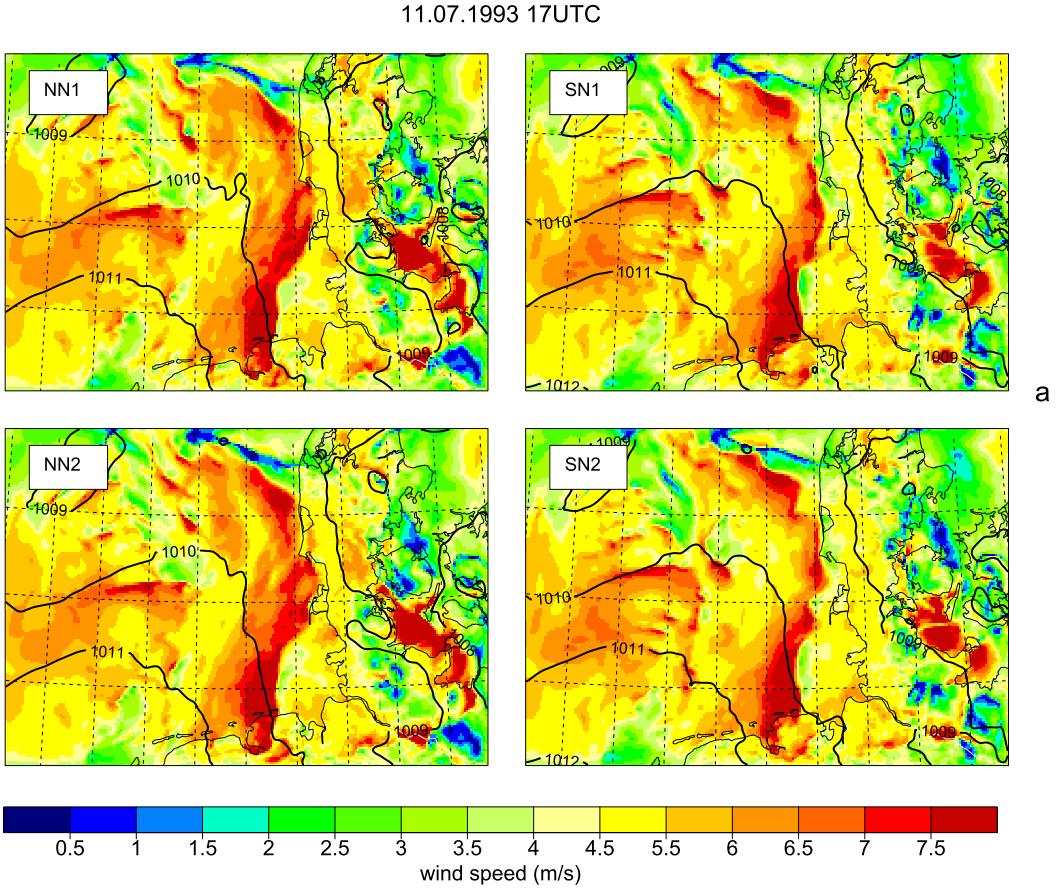

FIG. 4. Pressure isobars [(top left) NN_1, (bottom left) NN_2, (top right) SN_1, and (bottom right) SN_2] for (a) 1700 UTC 11 Jul 1993, (b) 0000 UTC 11 Mar 1993 (with shaded wind speed fields), and (c) 0400 UTC 23 May 1993 (with shaded precipitation fields).

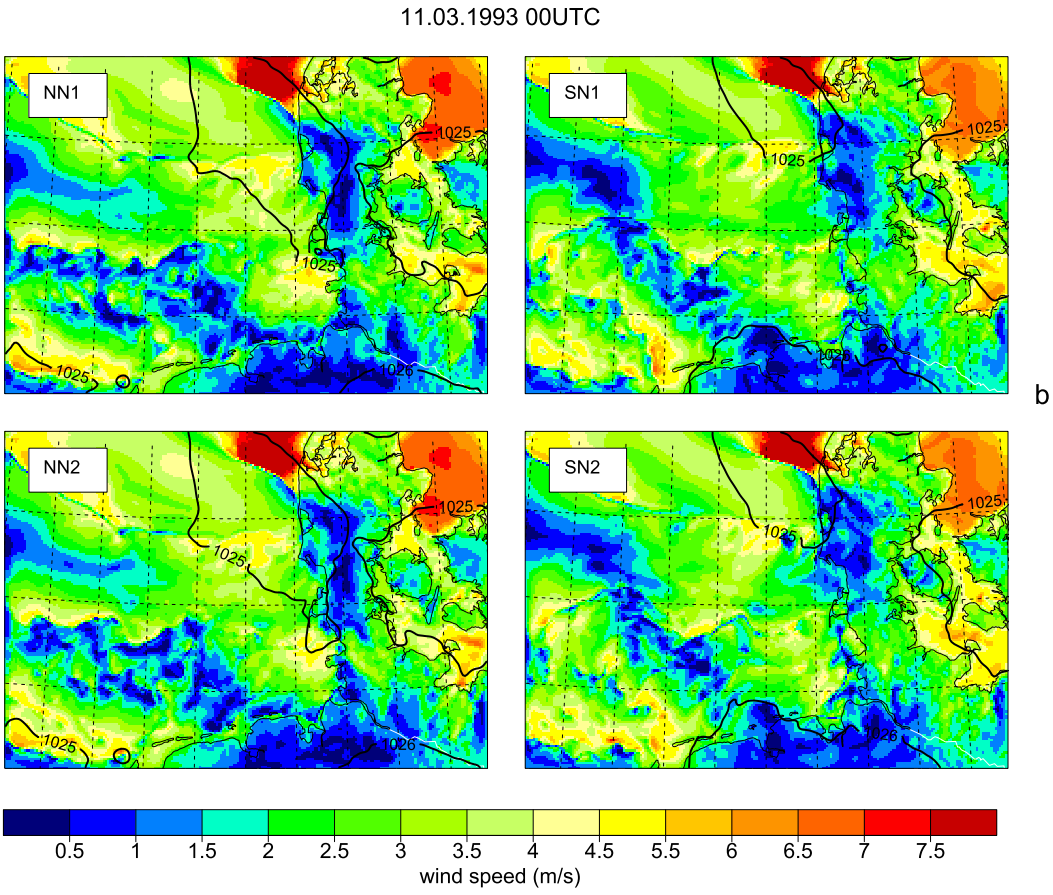

FIG. 4. (*Continued*)

difference in the initial conditions is sufficient to generate intermittent differences between the individual ensemble members for various variables in the large domain setup (Weisse et al. 2000; Weisse and Feser 2003).

In the two SN runs, only scales shorter than 80 km are unconstrained (i.e., wavenumber 9 and above in zonal directions are subject to spectral nudging, and wavenumber 6 and above in meridional directions). Spectral nudging was applied every third time step with a nudging factor of 0.5.

b. Evaluation strategy

The data from the SN and NN simulations are available hourly, and are thus markedly correlated in time, and the tests become liberal (the null hypothesis is much more often rejected than stipulated by the normal risk level). To avoid this, we use all data to calculate the differences, but use a critical value valid for 122 samples, corresponding to one value every three days. This approach, mimicking the use of real degrees of freedom in *t* tests (Zwiers and von Storch 1995), is expected to overcome the problem of serial autocorrelation.

We then calculate a number of statistics of these difference fields, and examine three episodes, when we find relatively large NN–SN differences in terms of synoptic similarity and regional detail. It turns out that there are hardly any differences at the synoptic scale, quite differently from the large-domain case of von Storch et al. (2000), but that the differences in precipitation are regionally large, in particular at the gridpoint scale.

3. Results

a. Ensemble variability of the SN and NN runs

In this section we investigate the similarity of the SN_1 and SN_2 simulation as well as the similarity of the NN_1 and NN_2 simulation. Analyzed were 10-m and 500-hPa scalar wind speed (WSS), 2-m temperature (T_2M), precipitation (TOT_PREC), and sea level pressure (PMSL). We also analyzed the meridional and zonal 10-m wind speed separately, but found that they behave just like the 10-m wind speed, so we do not show these variables separately in the study. Figure 1 also

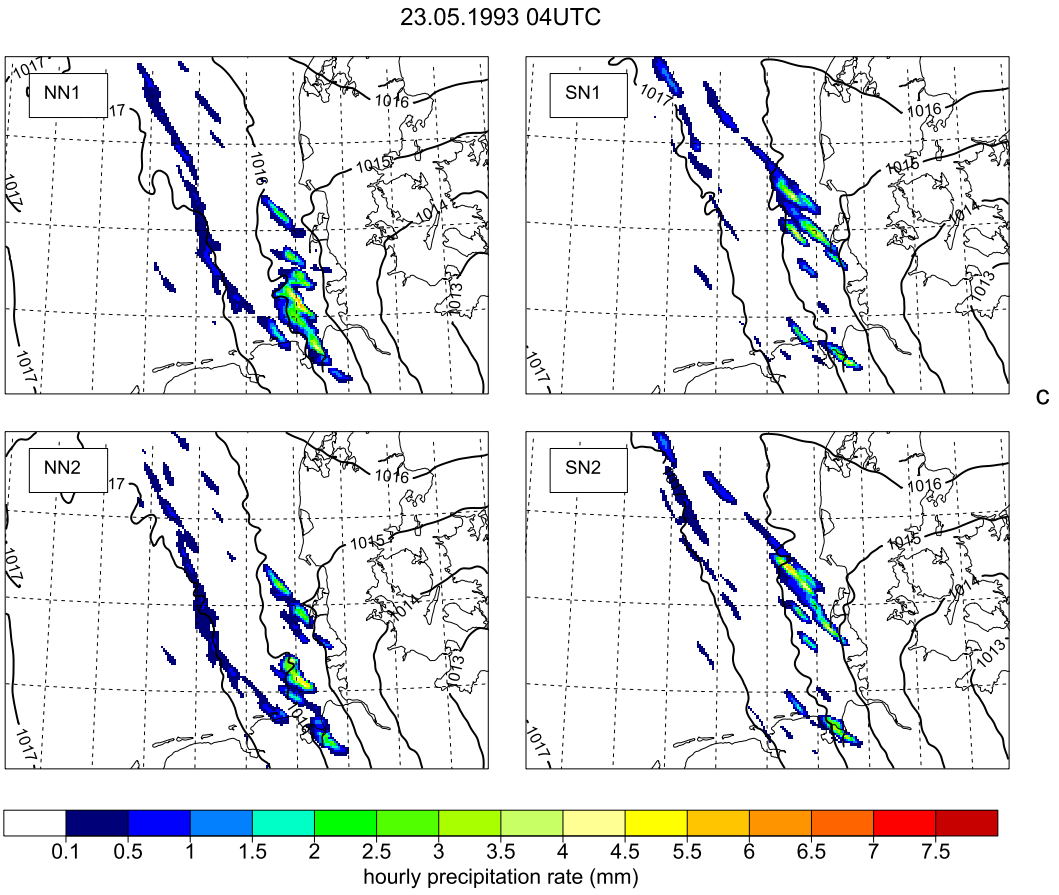

FIG. 4. (*Continued*)

shows the tracks of storm Verena, which occurred in January 1993. The tracks were determined with a simple tracking algorithm (Feser and von Storch 2008) on the basis of sea level pressure and near-surface wind speed. The tracks of the SN runs are exactly identical, as well as the tracks of the NN runs. The SN and NN tracks are almost identical and differ no more than 17 km.

The root-mean-square error (RMSE) is calculated spatially for every time step and is given by

$$\mathrm{RMSE} = \sqrt{\frac{1}{n}\sum_{i=1}^{n}(x_i - y_i)^2},$$

where x and y are the modeled variables of simulations 1 and 2. The index n is the total number of grid points in the model domain. Subsequently we plotted the cumulated distribution function of the whole analyzed year (one dot for every time step). These distribution functions of the RMSE between NN_1 and NN_2, and between SN_1 and SN_2 are again very similar for 10-m wind speed (Fig. 2). Precipitation and 2-m temperature show the same behavior as the 10-m wind speed and the SN and NN curves do not differ (not shown). For sea level pressure and wind speed at 500 hPa the NN runs show slightly higher variability (i.e., RMSEs) than the SN simulations (Fig. 2). The reason for this behavior is that 500 hPa is a vertical level where spectral nudging takes place and sea level pressure is a height-integrated variable and, therefore, influenced by spectral nudging at higher levels. The Kolmogorov–Smirnov test (Conover 1971) assesses the differences between NN and SN as not statistically significant. But for sea level pressure and wind speed at 500 hPa, the two distribution functions support the hypothesis that the variability for SN is slightly smaller than for NN.

b. Differences between SN and NN simulations

For this comparison we choose the SN_1 and NN_1 simulation, because we showed in the previous section, that the differences between SN_1 and SN_2 are similar to the differences between NN_1 and NN_2. In Table 1 statistical values are presented for the NN_1–NN_2, SN_1–SN_2, and SN_1–NN_1 difference distributions. The distributions are all centered around 0, except the SN_1–NN_1

distribution for sea level pressure, which is shifted by 7 Pa. The absolute maximum values, 99th percentiles, and standard deviation (SD) are higher in the SN_1–NN_1 difference than in the other ones. The minimum pattern correlations during the whole year and the value of the grid point with the minimum time correlation are lower in the SN_1–NN_1 difference. But the correlations still show a very high similarity with values larger than 0.8 except for the precipitation in the time and pattern correlation and 500-hPa wind speed in the pattern correlation. The 10th percentile of the pattern correlation shows that the minimum values of the pattern correlation are rare exceptions.

The time series of the pattern correlation (Fig. 3) confirms that for all variables, except for 500-hPa wind speed and precipitation, the correlation is larger than 0.8 at every time step. The pattern correlation of the 500-hPa wind speed shows a few cases with lower values between 0.8 and 0.4. The hourly precipitation pattern correlation (not shown) is close to 0 in many situations, but only for regionally restricted small precipitation amounts. For large precipitation areas there is a minimum correlation of 0.8. If only daily sums of precipitation are analyzed, the small spatial shifts of precipitation and the low pattern correlations of certain time steps are reduced. This leads to an increase of the pattern correlation to more than 0.5 for nearly all days, except for some days especially in early summer. In Figs. 4a and 4b sea level pressure and the 10-m wind speed maps are shown for times of minimum pattern correlation between SN_1 and NN_1 for 11 July 1993, which featured a minimum for 10-m wind speed correlation and 11 March 1993, with a minimum sea level pressure correlation (see Table 1). The date of the minimal sea level pressure pattern correlation is the same as in the von Storch et al. (2000) study. But in this study there are only some small differences in the pressure field, but no large-scale deviations like the ones shown in the von Storch et al. (2000) study (differences of more than 15 hPa). It is a stable high pressure situation, in which the air mass can remain longer in the model domain than for weather situations such as strong westerlies and thus there is more time for the RCM to develop large-scale variations, which cause smaller, but still very high, pattern correlations. The wind field at the date of the minimum pattern correlation of the 10-m wind speed shows some different structures, especially in regions with calm winds. As an example for low precipitation correlation, Fig. 4c shows a situation with small isolated spots of precipitation. The pattern correlation between SN_1 and NN_1 is 0.145. The location of the main precipitation is shifted southward in the NN_1 simulation. The results show that precipitation is a very nondeterministic variable, as there are also larger differences between the precipitation fields of NN_1 and NN_2 than in the fields of the other investigated atmospheric variables. The two SN precipitation fields are more similar to each other. If only daily sums of precipitation are analyzed, the small spatial shifts of precipitation and the low pattern correlations of certain time steps are reduced. This leads to an increase of the pattern correlation to more than 0.7 for nearly all days.

The comparison between SN_1 and NN_1 shows larger differences than between SN_1 and SN_2 and between NN_1 and NN_2, especially for precipitation, but also for all other variables. We suggest that the state, which is strived for by the model, is slightly different from the state of the RCM using spectral nudging.

c. *Comparison with observations*

A comparison with observation was performed in order to analyze the quality of the simulations with and without spectral nudging. Figure 5 shows the distribution function of the RMSE between the SN or NN simulations and observations of the German Weather Service. Wind speed and sea level pressure observations were available hourly; precipitation was available daily. Both distribution functions are nearly identical for all variables. The bias relative to observations is about as large for the NN runs as for the SN runs. The Kolmogorov–Smirnov test (5% error probability) cannot reject the null hypothesis that the SN-RMSE is larger than or equal to the NN-RMSE, so the differences between the NN and SN are not statistically significant.

4. Summary and discussion

In this short article, we examined the effect of spectral nudging on regional climate model results when using very small model domains, which are often used nowadays for very high convection-permitting resolutions due to high computing time costs. Both SN simulations show negligible differences for all analyzed variables. Even both NN simulations do not show noteworthy differences, though they lack the spectral nudging control within the model domain. We conclude that the ensemble variability of spectral nudging for the surface variables 10-m wind speed and precipitation has the same negligible magnitude like the ensemble variability without spectral nudging for the domain size of about 700 km × 500 km. The ensemble variability of the runs without spectral nudging for wind speed at 500 hPa is higher, because at this pressure level spectral nudging takes place in the SN runs. A similar effect on sea level pressure, a height-integrated variable, is detected.

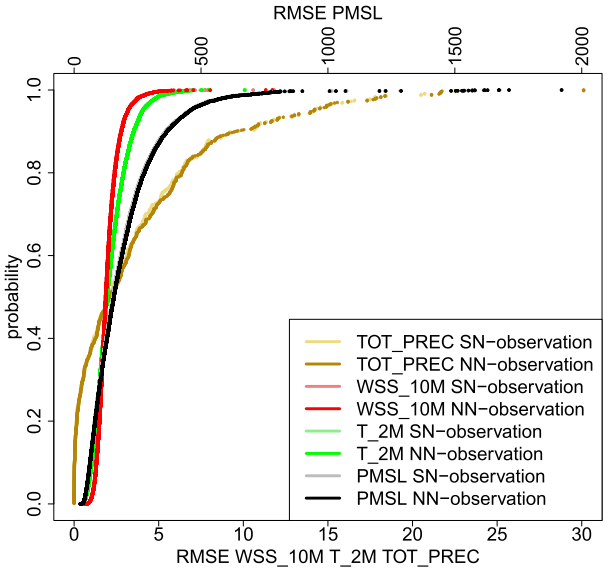

FIG. 5. Distribution function of the RMSE between SN and observations (light colors) and between NN and observations (dark colors) for 10-m wind speed (WSS_10M), total precipitation (TOT_PREC), 2-m temperature (T_2M), and sea level pressure (PMSL).

With spectral nudging, nearly the same state is produced independently of the starting date, which is the initial idea of spectral nudging. But also for the simulation without spectral nudging the model produces very similar states and fields at various starting dates, which is not the case for larger domain sizes (Alexandru et al. 2009). Even though the high-resolution RCM features a high number of model grid points, the region is still small in absolute dimensions. An air parcel will quickly cross the model domain and will be largely influenced by its values at the inflowing model boundaries. This implies that the size of the domain is too small to develop large-scale variations and the lateral boundary conditions are sufficient to force the atmospheric state into a similar state.

The temporal and spatial states of the two ensembles with and without spectral nudging are nearly identical. But the state, which is developed by the model without spectral nudging, is slightly different from the state of the RCM using spectral nudging. All simulations employ the same lateral and lower boundary conditions, but the SN runs use in addition spectral nudging at higher model levels inside the model domain, which seems to lead to marginally different weather states. It is conceivable that these differences result from different model versions, which were used for the sensitivity study and for the simulation of the forcing data coastDat, which is also used for the spectral nudging. Also different settings, which are necessary for different resolutions, could cause these discrepancies. But generally the SN and NN simulations are very similar for most variables with correlations larger than 0.8. Only precipitation shows pattern correlations smaller than 0.3 at certain times. These small correlations usually occur in situations with very weak precipitation with an hourly precipitation rate smaller than $1\,\mathrm{l\,m^{-2}}$ in the model domain (see Fig. 4c, pattern correlation of only 0.145 between SN_1 and NN_1). When daily precipitation sums are taken into account, the pattern and time correlation increases to values of more than 0.7. Comparisons with observations showed that the simulations with spectral nudging are not closer to station data than the ones without spectral nudging.

In this study we demonstrated that spectral nudging is not necessary for small RCM domain sizes of only several hundred kilometers in diameter and over flat and homogeneous terrain. The experiment is limited because of the small number of simulations of only four simulations (two ensembles with spectral nudging and two ensembles without spectral nudging). The results suggest that a higher number of ensemble members would have given similar results, but this should be analyzed in more detail in the future. What remains to be done for the future are further systematic tests with various domain sizes over different orographic terrains and geographical regions in order to determine threshold domain sizes from which spectral nudging becomes essential.

Acknowledgments. The work was supported through the Cluster of Excellence "CliSAP" (EXC177), Universität Hamburg, funded through the German Research Foundation (DFG). It is a contribution to the Helmholtz Climate Initiative REKLIM (Regional Climate Change), a joint research project of the Helmholtz Association of German research centers (HGF). The German Climate Computing Center (DKRZ) provided the computer hardware for the regional climate model simulations in the project "Storms." We are grateful to Beate Geyer for the coastDat II dataset. The German Weather Service (DWD) supplied observation data.

REFERENCES

Alexandru, A., R. de Elia, R. Laprise, L. Separovic, and S. Biner, 2009: Sensitivity study of regional climate model simulations to large-scale nudging parameters. *Mon. Wea. Rev.*, **137**, 1666–1686, doi:10.1175/2008MWR2620.1.

Castro, C. L., R. A. Pielke Sr., and G. Leoncini, 2005: Dynamical downscaling: Assessment of value retained and added using the Regional Atmospheric Modeling System (RAMS). *J. Geophys. Res.*, **110**, D05108, doi:10.1029/2004JD004721.

Caya, D., and S. Biner, 2004: Internal variability of RCM simulations over an annual cycle. *Climate Dyn.*, **22**, 33–46, doi:10.1007/s00382-003-0360-2.

Christensen, O. B., M. A. Gaertner, J. A. Prego, and J. Polcher, 2001: Internal variability of regional climate models. *Climate Dyn.*, **17**, 875–887, doi:10.1007/s003820100154.

Conover, W. J., 1971: *Practical Nonparametric Statistics*. John Wiley & Sons, 295–301, 309–314.

Davies, H. C., 1976: A lateral boundary formulation for multi-level prediction models. *Quart. J. Roy. Meteor. Soc.*, **102**, 405–418, doi:10.1002/qj.49710243210.

Deque, M., S. Somot, E. Sanchez-Gomez, C. M. Goodess, D. Jacob, G. Lenderink, and O. Christensen, 2012: The spread amongst ENSEMBLES regional scenarios: Regional climate models, driving general circulation models and interannual variability. *Climate Dyn.*, **38**, 951–964, doi:10.1007/s00382-011-1053-x.

Feser, F., and H. von Storch, 2008: A dynamical downscaling case study for typhoons in SE Asia using a regional climate model. *Mon. Wea. Rev.*, **136**, 1806–1815, doi:10.1175/2007MWR2207.1.

——, and M. Barcikowska, 2012: The influence of spectral nudging on typhoon formation in regional climate models. *Environ. Res. Lett.*, **7**, doi:10.1088/1748-9326/7/1/014024.

——, B. Rockel, H. von Storch, J. Winterfeldt, and M. Zahn, 2011: Regional climate models add value to global model data: A review and selected examples. *Bull. Amer. Meteor. Soc.*, **92**, 1181–1192, doi:10.1175/2011BAMS3061.1.

Geyer, B., 2014: High-resolution atmospheric reconstruction for Europe 1948–2012: coastDat2. *Earth Syst. Sci. Data*, **6**, 147–164, doi:10.5194/essd-6-147-2014.

——, and B. Rockel, 2013: coastDat-2 COSMO-CLM atmospheric reconstruction. World Data Center for Climate, DKRZ, accessed January 2017, doi:10.1594/WDCC/coastDat-2_COSMO-CLM, http://cera-www.dkrz.de/WDCC/ui/Compact.jsp?acronym=coastDat-2_COSMO-CLM.

Giorgi, F., and X. Bi, 2000: A study of internal variability of a regional climate model. *J. Geophys. Res.*, **105**, 29 503–29 521, doi:10.1029/2000JD900269.

Laprise, R., and Coauthors, 2012: Considerations of domain size and large-scale driving for nested regional climate models: Impact on internal variability and ability at developing small-scale details. *Climate Change*, A. Berger, F. Mesinger, and D. Sijacki, Eds., Springer, 181–199, doi:10.1007/978-3-7091-0973-1_14.

Lucas-Picher, P., D. Caya, R. de Elia, and R. Laprise, 2008: Investigation of regional climate models' internal variability with a ten-member ensemble of 10-year simulations over a large domain. *Climate Dyn.*, **31**, 927–940, doi:10.1007/s00382-008-0384-8.

Prein, A. F., and Coauthors, 2015: A review on regional convection-permitting climate modeling: Demonstrations, prospects, and challenges. *Rev. Geophys.*, **53**, 323–361, doi:10.1002/2014RG000475.

Rockel, B., C. L. Castro, R. A. Pielke Sr., H. von Storch, and G. Leoncini, 2008a: Dynamical downscaling: Assessment of model system dependent retained and added variability for two different regional climate models. *J. Geophys. Res.*, **113**, D21103, doi:10.1029/2007JD009461.

——, A. Will, and A. Hense, 2008b: The Regional Climate Model COSMO-CLM (CCLM). *Meteor. Z.*, **17**, 347–348, doi:10.1127/0941-2948/2008/0309.

Separovic, L., S. Z. Husain, and W. Yu, 2015: Internal variability of fine-scale components of meteorological fields in extended-range limited-area model simulations with atmospheric and surface nudging. *J. Geophys. Res. Atmos.*, **120**, 8621–8641, doi:10.1002/2015JD023350.

Steppeler, J., G. Doms, U. Schättler, H. W. Bitzer, A. Gassmann, U. Damrath, and G. Gregoric, 2003: Meso-gamma scale forecasts using the nonhydrostatic model LM. *Meteor. Atmos. Phys.*, **82**, 75–96, doi:10.1007/s00703-001-0592-9.

von Storch, H., H. Langenberg, and F. Feser, 2000: A spectral nudging technique for dynamical downscaling purposes. *Mon. Wea. Rev.*, **128**, 3664–3673, doi:10.1175/1520-0493(2000)128<3664:ASNTFD>2.0.CO;2.

Weisse, R., and F. Feser, 2003: Evaluation of a method to reduce uncertainty in wind hindcasts performed with regional atmosphere models. *Coast. Eng.*, **48**, 211–225, doi:10.1016/S0378-3839(03)00027-9.

——, H. Heyen, and H. von Storch, 2000: Sensitivity of a regional atmospheric model to a sea state-dependent roughness and the need for ensemble calculations. *Mon. Wea. Rev.*, **128**, 3631–3642, doi:10.1175/1520-0493(2000)128<3631:SOARAM>2.0.CO;2.

Zhao, Y., D. Wang, Z. Liang, and J. Xu, 2016: Improving numerical experiments on persistent severe rainfall events in southern China using spectral nudging and filtering schemes. *Quart. J. Roy. Meteor. Soc.*, **142**, 3115–3127, doi:10.1002/qj.2892.

——, ——, and J. Xu, 2017: Improving the regional model forecasting of persistent severe rainfall over the Yangtze River Valley using the spectral nudging and update cycle methods: A case study. *Atmos. Sci. Lett.*, **18**, 96–102, doi:10.1002/asl.731.

Zwiers, F., and H. von Storch, 1995: Taking serial correlation into account in tests of the mean. *J. Climate*, **8**, 336–351, doi:10.1175/1520-0442(1995)008<0336:TSCIAI>2.0.CO;2.